Centro Euro-Mediterraneo sui Cambiamenti Climatici

Technical Notes
April 2021
Issue 0290

CSP -Climate Simulations and Predictions Division

Tuning of some orography-related drag parameterizations in the atmospheric component of the CMCC Operational Seasonal Prediction Systems

By ***Guido Davoli***
University Ca' Foscari Venice
guido.davoli@unive.it

Stefano Tibaldi
Fondazione Centro Euro–Mediterraneo sui Cambiamenti Climatici
stefano.tibaldi@cmcc.it

Antonella Sanna
Fondazione Centro Euro–Mediterraneo sui Cambiamenti Climatici
antonella.sanna@cmcc.it

Marianna Benassi
Fondazione Centro Euro–Mediterraneo sui Cambiamenti Climatici
marianna.benassi@cmcc.it

Andrea Borrelli
Fondazione Centro Euro–Mediterraneo sui Cambiamenti Climatici
andrea.borrelli@cmcc.it

Antonio Cantelli
Fondazione Centro Euro–Mediterraneo sui Cambiamenti Climatici
antonio.cantelli@cmcc.it

Maria Chaves Montero
Fondazione Centro Euro–Mediterraneo sui Cambiamenti Climatic i
mariadm.chaves@cmcc.it

Silvio Gualdi
Fondazione Centro Euro–Mediterraneo sui Cambiamenti Climatici
silvio.gualdi@cmcc.it

SUMMARY Starting from October 1st, 2020, a new version of the Euro-Mediterranean Center on Climate Change Seasonal Prediction System (CMCC-SPS3.5) has been made operational at CMCC, producing each month global seasonal forecasts for a variety of users, including the Copernicus Multi-Model Seasonal Prediction System. CMCC-SPS3.5 has replaced the previous system version CMCC-SPS3. In both systems, the atmospheric, land surface, sea ice and river routing model components are based on CESM, the NCAR Community Earth System Model version 1.2.2, while the ocean component is based on NEMO, the Nucleus for European Modelling of the Ocean model, in its 3.4 version. The new version of the Seasonal Prediction System differs from the previous one essentially only for the horizontal resolution of the atmospheric model component (CAM 5.3), doubled from approximately 1° in SPS3 to approximately 0.5° in SPS3.5. Due to this doubling of the atmospheric model horizontal resolution, re-tuning some physical parametrizations of the atmospheric model was considered useful in order to reduce the model bias, mostly on the zonal flow and lower and mid-tropospheric, mid-latitude dynamical fields. The re-tuning effort was based on the results of a number of 5-year AMIP-like simulations (1981-1985) and it did concentrate on the parameterizations of Turbulent Orographic Form Drag, Orographic Gravity Wave Drag and Vertical Diffusion. Each of these parameterizations schemes has considerable influence on vertical momentum (and energy) transport and they all strongly interact non linearly with each other via, among other things, changing the mean flow. They cannot, therefore, be re-tuned singularly. Several combinations of the three parametrization settings were tried until a satisfactory set of new parameters was achieved, showing noticeable improvements in comparison with both the old SPS3 and the un-tuned SPS3.5 configurations, in particular over Europe during winter. This exercise underlines the importance of climate models' tuning when models' characteristics are changed, and how an increase in horizontal resolution alone, without an appropriate re-tuning, can create unbalances and even increase model biases.

Keywords Atmospheric modelling, parametrizations, bias reduction.

1. INTRODUCTION

The Euro-Mediterranean Center on Climate Change has been a regular producer of operational Seasonal Forecasts since 2013. In 2018 it started providing its forecasts, produced with the CMCC-SPS3 System, to the EU Copernicus Programme as one of the Multi-Model Seasonal Forecasting components, together with ECMWF, UKMO, Meteo-France and DWD. In October 2020, the SPS3 System was replaced by the new System version SPS3.5, with a doubled horizontal resolution of the atmospheric model component, from 1° x 1° to ½° x ½°. In view of the operational implementation of this doubling of the atmospheric model horizontal resolution, a re-tuning of some physical parametrizations of the atmospheric model was considered useful in order to address the problem of the model bias, concentrating the attention mostly on winter, mid-latitude dynamical fields. It has long been known that a typical feature of NWP and Climate (atmospheric) model bias is associated to their inability to correctly represent the intensity and the structure of the zonal flow, and that the representation of orographic effects is one (by any means not the only) of the related sources of inaccuracy (Wallace et al., 1983; Tibaldi, 1986; Palmer et al., 1986; Berckmans et al., 2013; Pithan et al., 2016; Sandu et al. 2019). Since model horizontal resolution plays an important role in determining the correct dissipation levels of momentum and energy, for example via the various types of drag exerted on the mean flow by orographic features/effects either explicitly resolved or unresolved (and therefore parametrized, Brown, 2004; van Niekerk et al., 2016; Vosper et al., 2016), it was decided to spend some effort in retuning, in the increased resolution model, two important orographic drag parametrizations: Turbulent Orographic Form Drag (TOFD) and Orographic Gravity Wave Drag (OGWD) and, furthermore, the parameterization of Vertical Diffusion (VDIFF), which plays a very important role in re-distributing in the vertical dissipative effects on the westerlies. The paper will describe the CMCC-SPS Forecasting System as a whole and the Atmospheric Model in some more detail (Section 2), the parametrization schemes involved in the

retuning and the actual tuning performed (Section 3) and the overall effects of the retuning on the atmospheric model bias (Section 4). Section 5 will be devoted to some concluding remarks.

2. THE CMCC SEASONAL PREDICTION SYSTEM

The CMCC Seasonal Prediction System (CMCC-SPS) consists of several independent but fully coupled model components which simulate simultaneously the evolution of Earth's atmosphere, ocean, land, sea ice and river routing, together with a central coupler/driver component that controls data synchronization and exchange between modules (see Figure 1).

Figure 1. General scheme of the CMCC-SPS3.5 fully coupled Seasonal Prediction System

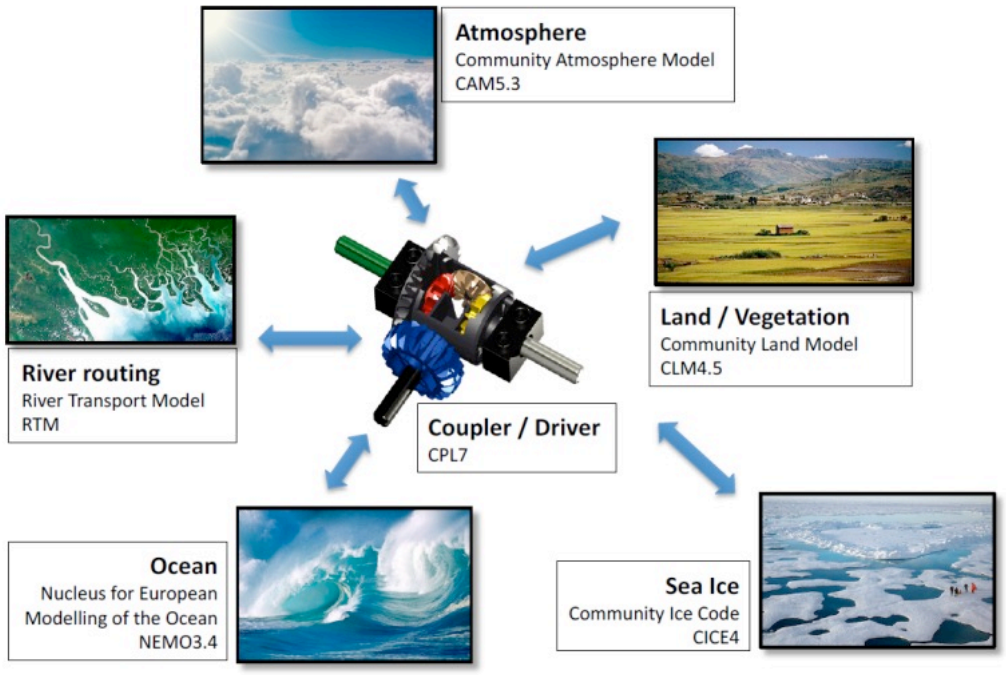

The CMCC-SPS atmospheric, land surface, sea ice and river routing model components are based on CESM, the NCAR Community Earth System Model version 1.2.2 (in their CAM5.3, CLM4.5, CICE4 and RTM versions, respectively). A detailed

description of such models is given in Hurrell et al. (2013) and references therein. The atmospheric model and the land model have a horizontal resolution of 1° x 1° (System version SPS3) or ½° x ½° (new System version SPS3.5). The ocean component of CMCC-SPS is based on NEMO, the European Nucleus for European Modelling of the Ocean model, in its eddy-permitting 3.4 version, with a horizontal resolution of ¼° x ¼° (Madec et al., 2008). In the horizontal, the model uses an ORCA, nearly isotropic, curvilinear, tri-polar, orthogonal grid, while in the vertical, a partial step z-coordinate is used, with 50 vertical levels. For an evaluation of CMCC-SPS3 performance in terms of climate bias and seasonal forecasting skill, see Sanna et al. (2017).

The atmospheric component of CMCC-SPS3.5 is the Community Atmosphere Model version 5 (CAM5.3, see Neale et al., 2012 for a description of the model macrophysics) which can be configured to use a spectral element, a finite volume, a spectral Eulerian or a spectral Semi-Lagrangian dynamical core, see Dennis et al. (2012) and Neale et al. (2012). The atmosphere implemented in CMCC-SPS3.5 is hydrostatic and uses the Spectral Element dynamical core (a formulation of the spectral element method using high-degree hybrid polynomials as base functions can be found in Patera, 1984), with a quasi-homogeneous horizontal resolution of ½° (about 55 km), 46 vertical levels up to about 0.3 hPa. The integration time-step of the full physics is 30 minutes (in both SPS3 and SPS3.5) while, as far as the dynamical core is concerned, the time-step of the “tracer” advection in SPS3.5 is 225 seconds (360 s in SPS3), i.e. 1/8 of the physics time-step (1/5 in SPS3) and the time-step of the fluid-dynamics is 56.25 seconds (90 s in SPS3), i.e. 1/32 of the physics time-step (1/20 in SPS3). The atmospheric model’s horizontal grid is the so-called Cubed-Sphere grid first used in Sadourny (1972). Each cube face is mapped to the surface of the sphere with the equal-angle gnomonic projection (Rancic et al., 1996) which amounts to tiling the surface of the sphere with quadrilaterals. An inscribed cube is projected to the surface of the sphere, then the faces of the cubed sphere are further subdivided to form a quadrilateral grid of the desired

resolution. The vertical coordinate is an eta-type coordinate, following Simmons and Burridge (1981).

Turning the attention to physical parametrizations, a description of the treatment for stratiform cloud formation, condensation, and evaporation macrophysics is given in Neale et al. (2012). A two-moment microphysics parameterization (Morrison and Gettelman, 2008; Gettelman et al. 2008) is used to predict the mass and number of smaller cloud particles (liquid and ice), while the mass and number of larger-precipitating particles (rain and snow) are diagnosed. A statistical technique is used to represent sub-grid-scale cloud overlap (Pincus et al., 2003). Cloud microphysics interacts with the model's greenhouse gas concentration, where observed yearly values are specified before 2005 and CMIP5 protocol concentrations (scenario RCP8.5) are used after 2005, see IPCC (2013). Differently from the standard version of CAM5.3, in CMCC-SPS3.5 (and in CMCC-SPS3) the aerosol distribution does not evolve in time but is taken from a fixed climatology (referring to the year 2000). The value of the total sun's radiative forcing (Solar Constant) is subjected to a solar cycle periodic variability and a Rapid Radiative Transfer Model for GCMs (RRTMG; Iacono et al., 2008, Bretherton et al., 2012, Liu et al., 2012) is used to calculate the radiative fluxes and heating rates for gaseous and condensed atmospheric species. Moist turbulence (Bretherton and Park, 2009) and shallow convection parameterization schemes (Park and Bretherton, 2009) are used to simulate shallow clouds in the planetary boundary layer. The process of deep convection is treated with a parameterization scheme developed by Zhang and McFarlane (1995) and modified with the addition of convective momentum transports by Richter and Rasch (2008) and a modified dilute plume calculation following Raymond and Blyth (1986, 1992). The physics package includes a parameterization of convective, frontal and orographic Gravity Wave Drag (GWD) following McFarlane (1987), Richter et al (2010) and Richter et al. (2014). The convective GWD efficiency is adjusted to produce a QBO period in the lower stratosphere closer to observations. The Turbulent Orographic Form Drag (TOFD) due to unresolved orography is taken into account by the

Turbulent Mountain Stress (TMS) scheme and details on this parameterization can be found in Neale et al. (2012), Richter et al. (2010) and Lindvall et al. (2017). Vertical Diffusion (VDIFF) of heat and momentum is parameterized following Bretherton and Park (2009) with the so-called "University of Washington Moist Turbulence scheme" (UWMT). Inside UWMT the effect of turbulence is represented by a down-gradient diffusion term. In the horizontal, a Hyperviscosity term is also included in order to damp the propagation of spurious grid-scale modes (Ainsworth & Wajid, 2009).

In its operational seasonal forecasting implementation, CMCC-SPS is operated in Ensemble mode (6-month predictions, 50 ensemble elements) and a set of hindcasts (re-forecasts) covering the 24-year period 1993-2016 (6-month predictions, 40 ensemble elements) has been produced for both SPS3 and SPS3.5 System versions. Initial condition (IC) fields for all necessary forecast modules (atmosphere, ocean, including sea ice, and land, including land ice and snow) are prepared routinely to initialize the monthly operational forecast. These IC fields are, furthermore, perturbed in order to generate the set of initial conditions to construct the ensemble. 10 atmospheric perturbed ICs, 3 land perturbed ICs and 9 (4 in hindcast mode) ocean perturbed ICs are combined to yield 270 perturbed ICs (120 in hindcast mode), among which 50 ICs (40 in hindcast mode) are chosen at random to produce the forecast ensemble.

3. THE MOUNTAIN-RELATED DRAG PARAMETRIZATIONS CONSIDERED FOR RETUNING

Before describing the effects of the retuning of the parameterizations on the model climate bias, a short description of the physical basis of the three schemes needs to be outlined and the three following sub sections are dedicated to this purpose.

All three parameterizations schemes considered have large influences on vertical momentum (and energy) transport and they strongly interact non linearly with each other via, among other things, changing the mean flow. They could not, therefore, be tuned one-by one, without taking into account the mutually interactive effects. Guidance in the

tuning effort was also derived by bearing in mind the order of application of the parameterizations in the numerical integration time-step cycle. The tendency due to TOFD on wind values is computed and applied first, and the effect of TOFD on the immediately successive application of OGWD can be very large, for example by decreasing the wind speed and therefore the possibility to successively generate orographic gravity waves (and thus decreasing the value of the tendency due to OGWD on wind itself). Several combinations of the three parametrization settings were therefore tried until a (subjectively) satisfactory set of new parameters was achieved, which showed noticeable improvements in comparison with both the old SPS3 and the un-tuned SPS3.5 configurations, in particular over Europe during winter. This is, admittedly, a somewhat arbitrary procedure, but a degree of arbitrariness is the only possibility in the absence of alternative prime-principle-based criteria and it is a procedure often used in parametrization tuning exercises.

At the end of each of the three following subsections, describing the parametrizations in some detail, the parameter value decided after the tuning effort is also reported, which is the one used in producing all the diagnostics material presented in Section 4.

3.1 TURBULENT OROGRAPHIC FORM DRAG (TOFD)

In CAM5, the turbulent surface drag due to unresolved orography is taken into account by the Turbulent Mountain Stress (TMS) scheme. Details on this parameterization can be found in Neale et al. 2012, Richter et al. 2010 and Lindvall et al. 2017.

The TMS surface stress τ is calculated as

$$\tau = \rho C_d |\mathbf{V}| \mathbf{V}$$

where ρ and V are the air density and the wind vector at the lowest model level and Cd is a drag coefficient given by

$$C_d = \frac{f(R_i) k^2}{\ln^2[(z + z_0)/z_0]}$$

where f(Ri) is a function of the Richardson number Ri of the form:

- f(Ri) = 1 if Ri < 0;
- f(Ri) = 0 if Ri > 1;
- f(Ri)= 1 – Ri if 0 < Ri < 1;

where k=0.4 is the Von Kàrmàn constant, z is the altitude of the model mean orography and z0 is an effective roughness length, representing the idealized size of the perturbing (turbulent-eddies-generating) surface elements due to the unresolved orography. In fact,

$$z_0 = \min (tms\_z0fac*\sigma , 100m)$$

where σ is the standard deviation of unresolved orography (measured in meters) on scales smaller than 6 km and assuming that the maximum vertical extent of the unresolved orographic roughness elements is order of 100m. Effects of the unresolved orographic spectrum on scales between 6 km and model resolution are taken into account by the gravity wave scheme (Sect. 3.1).

tms_z0fac is a numerical parameter affecting the minimum roughness length seen by the model. The standard value of tms_z0fac is 0.075. After the tuning experiments, it was decided to set tms_z0fac = 0.1875, increasing it by a factor 2.5.

The TMS scheme is active only over land points and only where surface altitude is greater than 0. In addition to TMS, the Community Land Model, coupled to CAM and also part of the CMCC-SPS Systems (see Fig.1), calculates the surface fluxes of momentum, sensible heat, and latent heat due to land cover (land use and vegetation), exploiting Monin-Obukhov similarity theory applied to the surface layer, Neale et al (2012) and Dai et al (2001). Over the ocean, surface fluxes of momentum, water and heat are diagnosed using bulk formulas documented in Neale et al (2012) and Bryan et al (1996).

3.2 OROGRAPHIC GRAVITY-WAVE DRAG (OGWD)

CAM5 OGWD is parameterized following McFarlane 1987. Further information can also be found in Neale et al. 2012.

The first quantity estimated by the parameterization scheme is the height of the source level at which orographic gravity waves are generated. This source level height is diagnosed as the depth to which the typical unresolved mountain penetrates into the atmosphere, which is taken to be equal to 2σ, where σ is the standard deviation of the unresolved orography on scales between 6 km and model horizontal resolution. The choice of this lower-limit cut-off length scale is motivated by the theoretical argument by which only sufficiently large orographic features are able to excite vertically propagating gravity waves. The effects of even smaller orographic feature on the atmospheric flow is taken into account by the form drag scheme (see next Section 3.2). Once the source level height is determined, the magnitude of the vertical flux of horizontal momentum at the source level (the stress) is parameterized as:

$$\tau_g = \frac{k}{2} h_0^2 \rho_0 N_0 \overline{u}_0$$

where h0 represent the streamline vertical displacement at the source level due to unresolved orography and ρ0, N0 and ū0 are the mean values of respectively air density, Brunt-Väisälä frequency and wind speed from the model lower surface up to the source level height. The streamline displacement h0 is also determined from the standard deviation of unresolved orography σ, and limited, following the saturation criterion proposed in McFarlane (1987), to avoid wave saturation at the source level in regions of large unresolved orographic standard deviation:

$$h_0 = \min\left[(2\sigma)^2, F_c \frac{\overline{u}_0}{N_0}\right]$$

where Fc is a critical inverse Froude number, set equal to 1 following theoretical arguments.

Once the stress at the source level stress calculated, the vertical profile of the vertical momentum flux is determined scanning all the model levels from the source level up to the model top. Physically, the aim of this procedure is to produce a vertical momentum flux that is constant where the wave does not experience dissipation processes, while it decreases with height in regions of wave breaking/saturation. Therefore, the vertical momentum flux at a given level k is assumed to be equal to the value at the level below, unless it is greater than a saturation value τ*.

In this case the vertical momentum flux is limited following the saturation criterion proposed by Lindzen 1981:

$$\tau_k \leq \tau^* = F_c^2 \frac{k}{2} \rho_k \frac{\overline{u}_k^3}{N_k}$$

and the algorithm proceeds to level above. The saturation value depends on local values of density, wind speed and Brunt-Väisälä frequency, and represents the residual momentum flux propagating upward after the wave experienced an instability. The whole stress profile is finally multiplied by an efficiency factor effgw_oro, crudely representing the effect of temporal and spatial intermittency of the wave breaking processes inside the model gridbox, an effect intuitively strongly dependent upon model horizontal resolution.

The second part of the code determines the wind tendency due to the drag force acting on the flow in regions of vertical momentum flux deposition due to wave dissipation, that is where the stress profile decrease with height. In fact, the stress profile is now scanned from the model top down to the source level, and the wind tendency at each level is determined differencing the stress profile between adjacent levels:

$$\frac{\partial \overline{u}_k}{\partial t} = g \frac{\delta^k \tau}{\delta^k p}$$

where p is pressure and $\delta^k X$ represents the difference between X at level k and X at the level below.

The magnitude of the momentum flux and, consequently, the value of wind tendencies are modulated by the efficiency parameter effgw_oro. Its standard value is 0.0625. After the tuning experiments, it was decided to increase, in the double resolution model, effgw_oro by a factor 2.5: in SPS3.5, effgw_oro = 0.15625.

3.3 VERTICAL DIFFUSION (VDIFF)

Vertical diffusion of heat and momentum in CAM5 is controlled by the Bretherton and Park (2009) parameterization, the "University of Washington Moist Turbulence scheme" (UWMT). Inside UWMT the effect of turbulence is represented by a downgradient diffusion; the turbulent fluxes of a variable X (heat, h, and momentum, m) between adjacent model levels are calculated as

$$\overline{w'\chi'} = -K_\chi \frac{\partial \chi}{\partial z}$$

where w indicates vertical velocity, z is height and the K_X, called eddy diffusivities, have the form

$$K_h = lS_h e^{1/2} \quad \text{and} \quad K_m = lS_m e^{1/2}.$$

Here, e is the local Turbulent Kinetic Energy (TKE), which is diagnosed by the scheme at each level interface; l is a turbulence length scale, and S_h and S_m are stability functions.

The Richardson number R is used to diagnose the existence of turbulence, and the activation of diffusion between adjacent levels. The transition between turbulent and stable level interfaces is marked by a critical Richardson number R_c: when $R>R_c$ the interface is labeled as stable, and diffusion does not happen, while if $R< R_c$ diffusion is

activated. Thus, after the classification based on the local Richardson number, the local e, l, S_h and S_m are calculated at turbulent interfaces, and the turbulent fluxes are estimated. The interested reader can find more details on the calculations in Bretherton and Park (2009).

The value of R_c in the untuned 0.5° Horizontral Resolution model version was 0.19. After the tuning experiments, we decided to nearly double R_c, setting R_c = 0.4, allowing therefore for more vertical diffusion.

4. THE EFFECTS OF THE TUNING ON THE ATMOSPHERIC MODEL BIAS

Having briefly outlined the three parametrizations which have been the object of the tuning effort, this section is devoted to documenting the effects of the tuning on the atmospheric model climate bias. As anticipated, all results are based upon 5-year AMIP-like model integrations covering the period 1981-1985, with the atmospheric model forced by observed SST and sea-ice conditions.

The effects of the three parametrizations retuning on the model climate bias will be documented by comparing mean fields of a number of atmospheric variables of the previously 1°x1° horizontal resolution model with the ½°x½° model, untuned and then tuned, and all of them with ERA5 reanalysis (Hersbach et al. 2020), remembering that no other change was made to dynamics or physics parameters (other than the necessary timesteps). All results refer mostly to the winter season (DJF) of the Northern Hemisphere. The layout of the figures/panels will, as far as possible, be mostly the same, with ERA5 full-field 5-year mean on the left, and then progressively towards the right the corresponding model bias of the 1° model (SPS3) and then the ½° model bias, first for the untuned model, then for the tuned model.

Starting from the MSLP field, it is evident from Fig. 2 that the horizontal resolution increase alone is having slightly negative effects on the MSLP bias, especially over Western Europe and the Eastern Atlantic, where the 1° model was already showing a negative bias centre over the North Atlantic. On the other hand, the bias is becoming

slightly worse over the North American continent and Northern Siberia, intensifying its Wavenumber 2 character.

Figure 2. Northern Hemisphere DJF MSLP. From left to right: ERA5 full field, 1° model bias, ½ ° untuned model bias, ½ ° tuned model bias. Integration period is December 1980-December 1985, included.

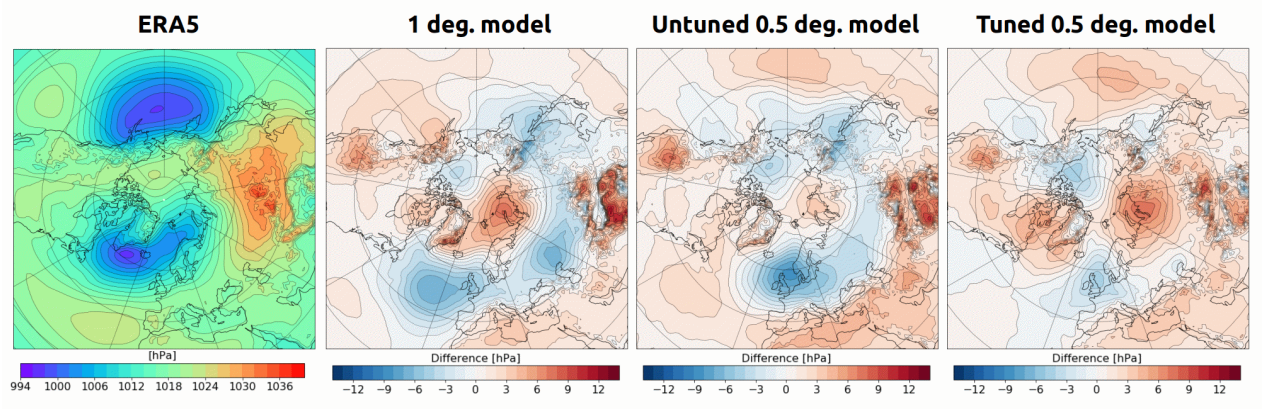

The 500 hPa Geopotential Height bias (Fig. 3) confirms the tendency, common to many global models, to show, compared with the MSLP maps, a bias characterized by a substantially equivalent-barotropic structure, with an evident Wavenumber 2 signature. The lower resolution model displays the largest bias, with a large negative centre over the North-Atlantic and a slightly less intense double negative structure over Northern Russia.

Figure 3. Northern Hemisphere DJF 500 hPa Geopotential Height. From left to right: ERA5 full field, 1° model bias, ½ ° untuned model bias, ½ ° tuned model bias. Integration period is December 1980-December 1985, included.

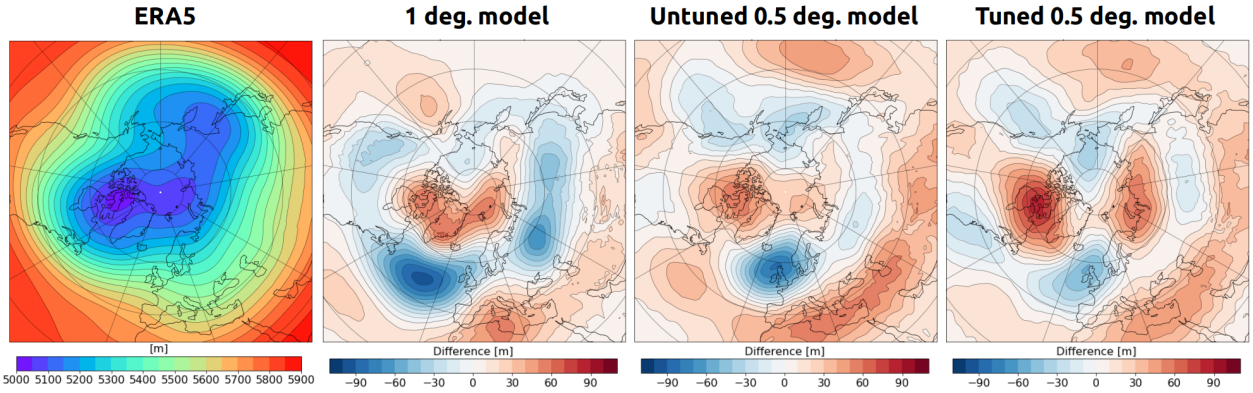

The untuned ½° model moves the main negative centre over the British Isles and Western Europe. This negative centre is much reduced by the retunin again with a strong WN2 signature g, at an expense, however, of the positive bias centres over Northern Siberia and North, America, again with a strong WN2 signature.

The comparison among models' biases of the Stationary Waves shown in Figure 4 allows to interpret the results of Figure 3, showing how the Stationary Waves bias is to be held responsible for the strong WN2 signature on the 500hPa (but not only) and for the mixed, somewhat contradictory, results of the retuning on the model's tropospheric NH mid-latitudinal winter climate bias.

Figure 4. Stationary Planetary Scale Waves bias at 500 hPa in the three model configurations. The panel arrangement is the same as in all other Figures.

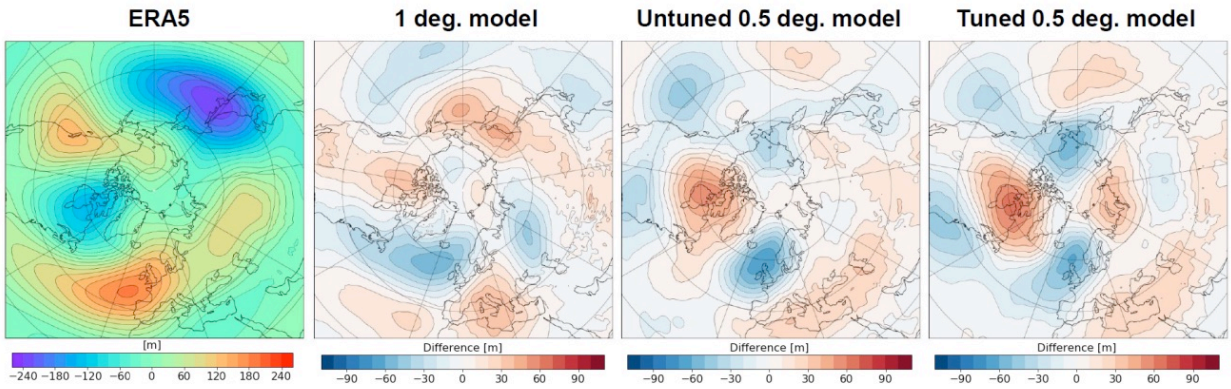

Turning the attention to mean westerly wind bias, Fig. 5 shows Northern Hemisphere DJF cross-sections of U for the whole Troposphere. All models show a similar pattern of NH westerly wind bias, with the mean westerly jet too strong and too concentrated in the mid-latitudes. The bias is essentially equivalent barotropic up to 200 hPa, where it tends to tilt equatorward. From this perspective, the positive impact of the retuning is very clear, since it reduces the bias with respect to both the 1° model and the ½° model, which shows an increase in the bias with the increase in horizontal resolution alone.

Figure 5. Northern Hemisphere DJF tropospheric cross-sections of U, the wind westerly wind component, Equator to 80°N. From left to right: ERA5, 1° model, ½ ° untuned model, ½ ° tuned model. Integration period is December 1980-December 1985, included.

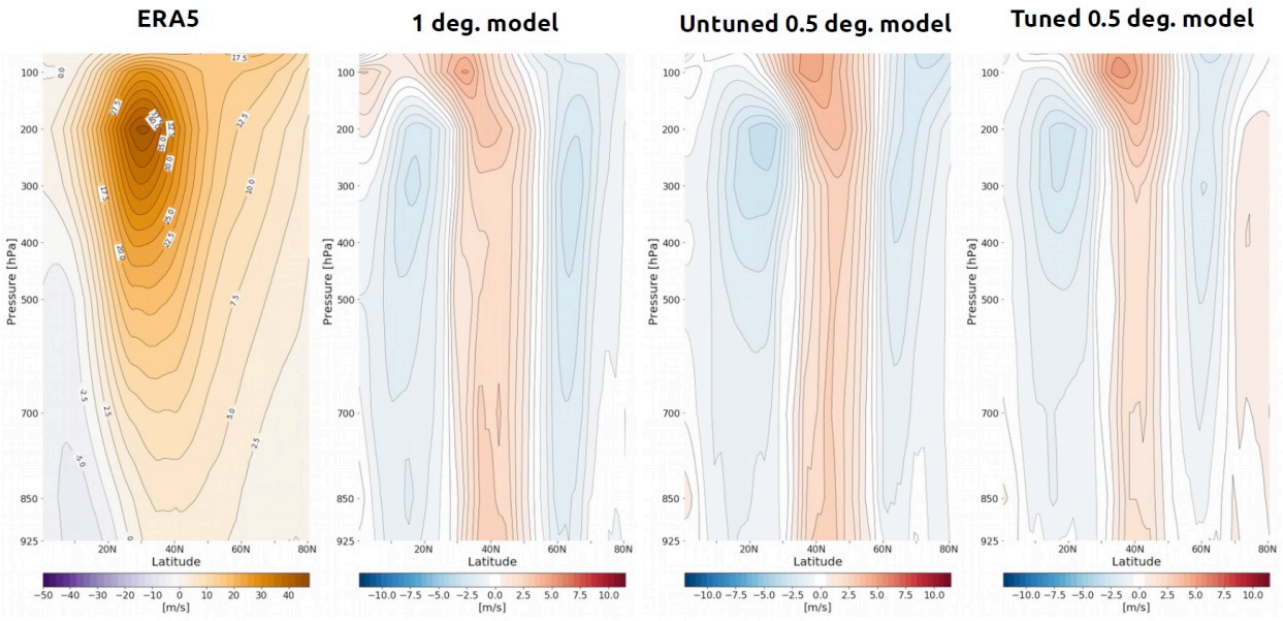

Figure 6 explores in some more detail the problem of the westerly wind bias by showing the Jet Latitude Index (Woollings et al. 2010), calculated from the zonal wind at 850 hPa over the Atlantic Sector (20N - 75N; 0W-60W) for the same DJF period, suggesting that the tuned, higher resolution model configuration is the only one capable of reducing the bias in jet intensity, without losing the capability to correctly represent the jet variability in latitudinal positioning which gives rise to the observed multi-modal latitudinal distribution. It should also be noted how the untuned ½° model erroneously concentrates the jet around 45°N even more than the 1° model, losing at the same time almost completely the two lateral secondary maxima at higher and lower latitudes.

Figure 6. Jet Latitude Index computed over the North Atlantic Sector (20N - 75N; 0W-60W) for ERA5, 1° Model, ½° untuned model and ½° tuned model (upper panel) and bias of all three models w.r.t. ERA5 (lower panel). Data are for Winter period (DJF)..

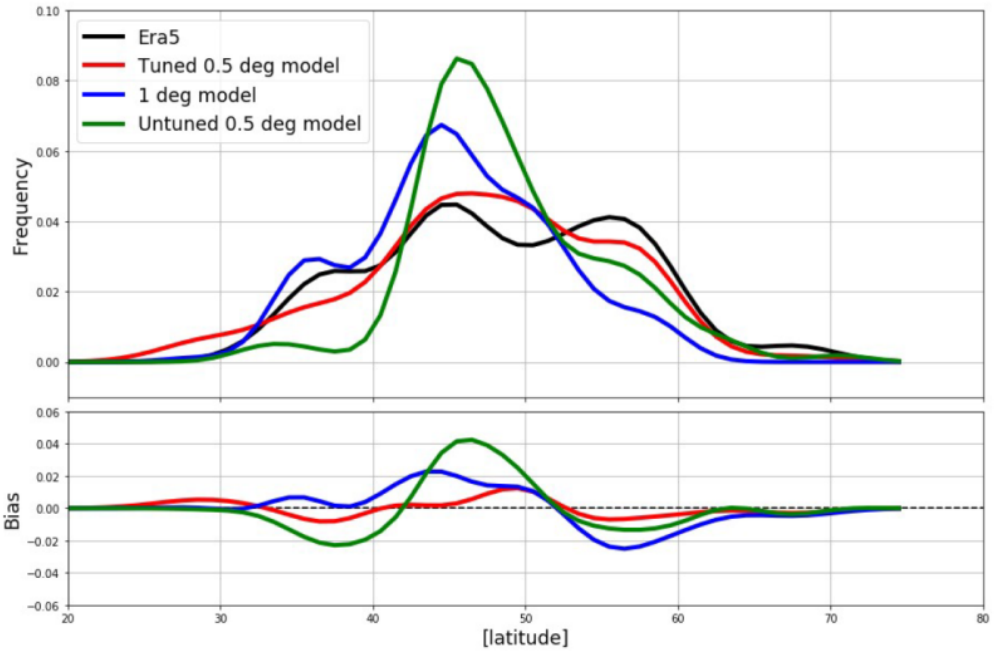

Figure 7. Northern Hemisphere DJF 850 hPa Zonal Wind. From left to right: ERA5 full field, 1° model bias, ½ ° untuned model bias, ½° tuned model bias. Integration period is December 1980-December 1985, included.

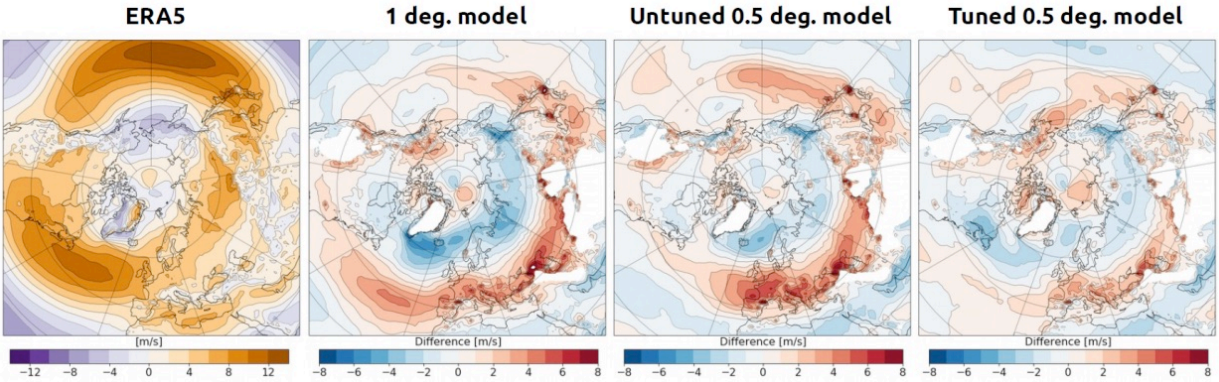

Figures 7 and 8 show the Northern Hemisphere, DJF Zonal Wind bias at 850 and 250 hPa. The equivalent-barotropic character of the error is clearly confirmed but, more interestingly, it is documented how the bias is more evident over the Atlantic and Eurasian sectors in the 1° model, over the Eurasian and Western Pacific sector in the ½° untuned model and is more evenly distributed around the hemisphere, in addition to being greatly reduced in amplitude, in the ½° tuned model, both at lower and high level. ½° untuned model and is more evenly distributed around the hemisphere, in addition to being greatly reduced in amplitude, in the ½° tuned model, both at lower and high level.

Figure 8. Northern Hemisphere DJF 250 hPa Zonal Wind. From left to right: ERA5 full field, 1° model bias, ½ ° untuned model bias, ½ ° tuned model bias. Integration period is December 1980-December 1985, included.

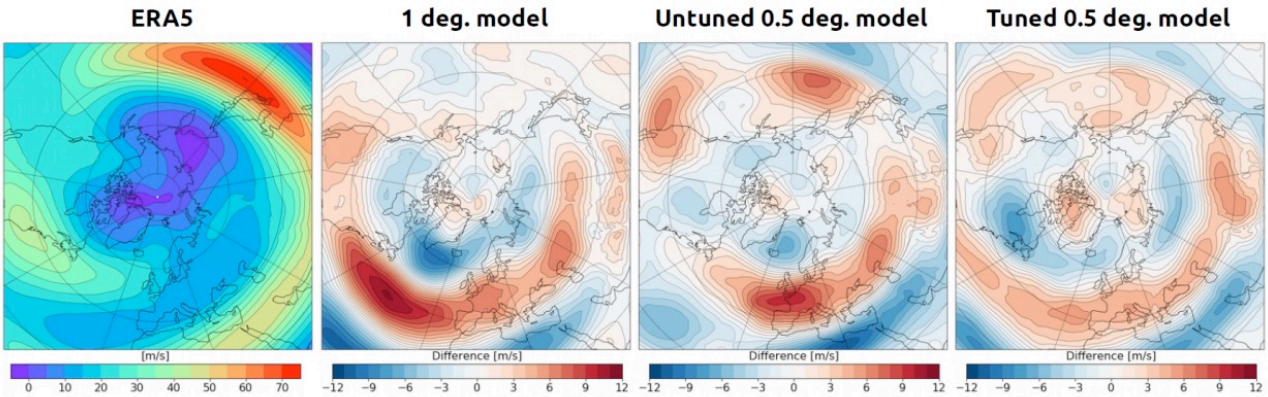

Figure 9 shows the global bias on precipitation. Here the effects of model resolution increase alone are slightly detrimental, especially over Indonesia and Northern Australia, and only the retuning effort is capable of reconducing the precipitation bias of the ½° model to values comparable to those of the 1° model, although not completely.

Figure 9. Global precipitation bias. Top left GPCP observations, top right 1° model, lower left untuned ½° model, lower right tuned ½° model.

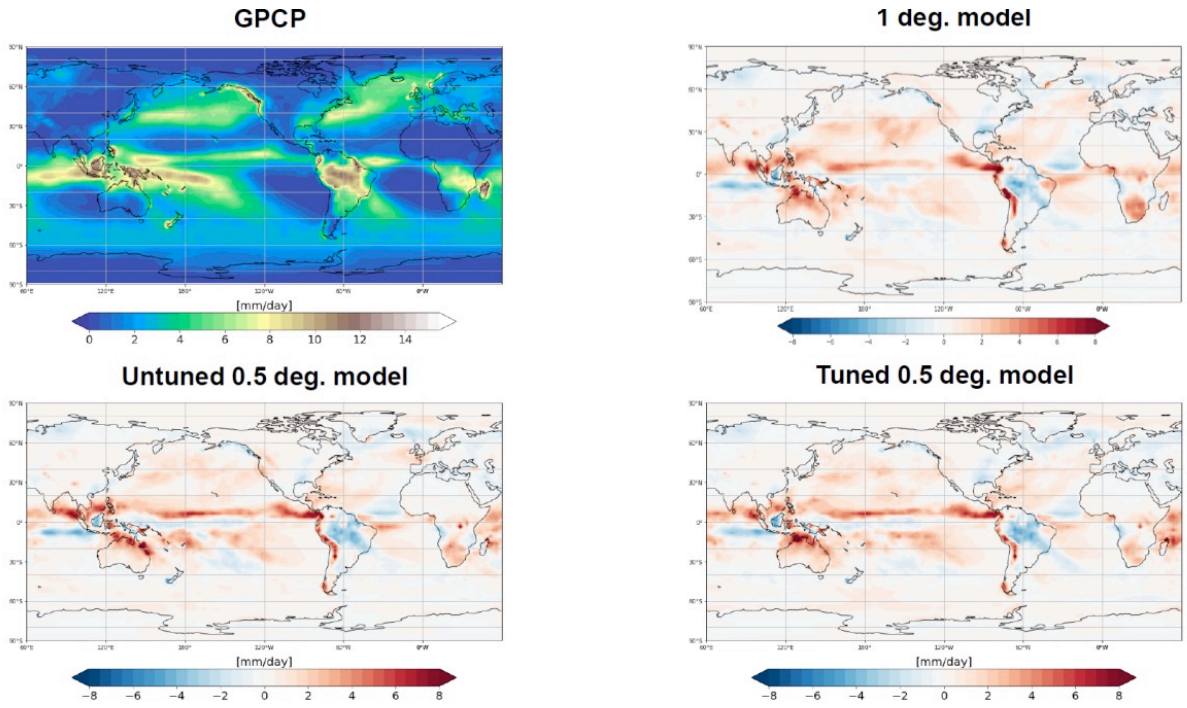

5. AN EXAMPLE OF PROCESS DIAGNOSTICS

In addition to comparing maps and cross-sections of mean fields of wind or geopotential height, it is of interest to verify the impact of the retuning on a dynamical processes considered to be of of great importance for the Northern Hemisphere mid-latitude winter troposphere: Atmospheric Blocking.

Atmospheric Blocking can be very synthetically described as a quasi-stationary, synoptic scale, high pressure pattern that establishes itself in some preferred quadrants of the Northern Hemispheric mid-latitudes, disrupting for a period of days-to-weeks the typical westerly progression of synoptic perturbations and thereby causing, by its

persistence, intense meteorological phenomena in the affected areas. See Tibaldi and Molteni (2017) and references therein for an overview of the process, associated phenomena, possible dynamical explanations and difficulties in modelling it. Since the early years of global operational medium-range numerical weather forecasts it has become apparent that representing blocking in numerical weather prediction models could constitute a problem (Tibaldi and Molteni, 1990), and the same was later found out for global climate models (e.g. D'Andrea et al, 1998). All of this explains why representing blocking has often been taken as a significant benchmark for global weather and climate model performance.

Figure 10 shows 2D maps of winter blocking frequency for ERA5, 1° model, ½° model untuned and tuned in the usual layout. Two facts appear evident: the resolution increase, far from being beneficial in this respect, decreases an already too low (as usual for weather and climate numerical models, e.g. Tibaldi and Molteni 1990; Jung et al 2010; Anstey et al., 2013; Davini and D'Andrea, 2020) blocking frequency, especially over Eastern Europe and Western Asia. The tuning is decisively beneficial, restoring more acceptable values of frequency over the high and mid-latitude belt which goes from the Western Atlantic all the way until Eastern Russia and Alaska, although the loss of the maximum over the Euro-Atlantic region evident from the comparison between the 1° and the ½° model panels is not completely recovered.

Figure 10. NH Winter Blocking Frequency computed with a two-dimensional blocking index (the "Absolute" method of Woolings et al., 2018) for the same five winters DJF period December 1980-February 1985. Panels layout as usual.

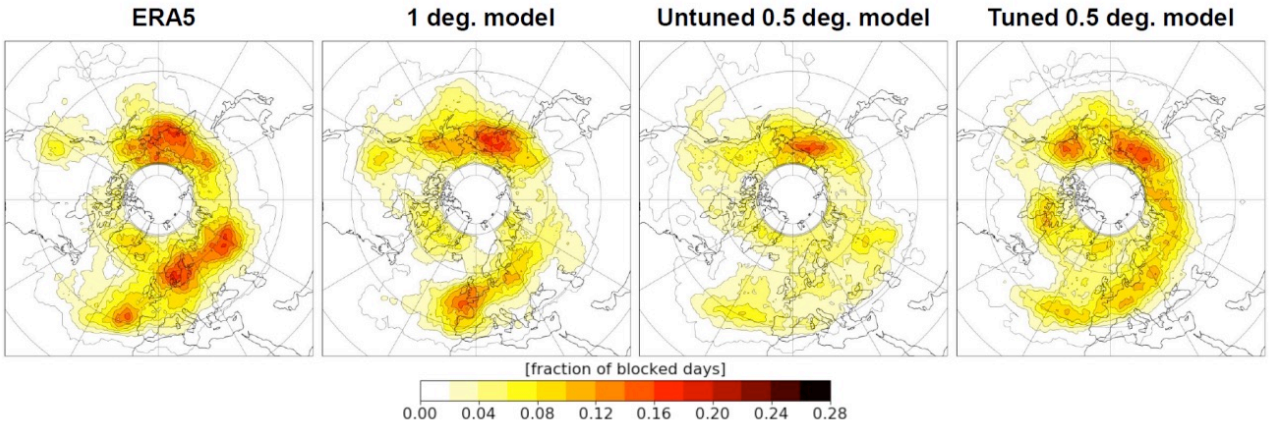

6. CONCLUSIONS

It is evident from the results shown that the mere increase of horizontal resolution does not, in itself, necessarily have a beneficial impact on the model's climate bias. This should not be a surprise, because many of the physical parametrization schemes are formulated in such a way as to be critically dependent on, at the same time, the volume of the grid-box and the exact values of the empirical parameters. The great importance, therefore, of an accurate retuning of all physics, and of orography-dependent parametrizations in particular, when atmospheric model horizontal resolution is changed, is clearly demonstrated.

The authors are aware that the work reported here paints an only partial picture of the effects of such a partial model physics re-tuning effort and therefore suffers from a number of shortcomings and limitations, possibly brought about by the urgency of implementing a higher resolution version of the CMCC operational model within a tight time schedule. The evidence reported about several final positive results of the effort, however, can be useful as a preliminary indication of possible directions to pursue in similar exercises to be performed by other modelling groups. The results documented here in any case underline the importance of climate models' physics re-tuning when models' characteristics are changed (in particular those which are strongly affected by model resolution). Care should therefore be applied when evaluating model intercomparison exercises based upon resolution increase alone, without previous appropriate physics re-tuning, since resolution increases alone could create undesirable effects due to unbalances and even increase model biases.

BIBLIOGRAPHY

Ainsworth, M., and Wajid, H. A. (2009). Dispersive and dissipative behavior of the spectral element method. *SIAM Journal on Numerical Analysis*, *47*(5), 3910–3937. https://doi.org/10.1137/080724976

Anstey, J. A., Davini, P., Gray, L. J., Woollings, T. J., Butchart, N., Cagnazzo, C., Christiansen, B., Hardiman, S. C., Osprey, S. M., and Yang, S. (2013). Multi-model analysis of Northern Hemisphere winter blocking: Model biases and the role of resolution, *J. Geophys. Res. Atmos.*, 118, 3956– 3971, *doi:10.1002/jgrd.50231*.

Berckmans, J., Woollings, T., Demory, M.-E., Vidale, P.-L. and Roberts, M. (2013). Atmospheric blocking in a high resolution climate model: influences of mean state, orography and eddy forcing. *Atmos. Sci. Lett., 14: 34-40. https://doi.org/10.1002/asl2.412*

Bretherton, C. S., and S. Park (2009). A new moist turbulence parameterization in the community atmosphere model, *J. Climate, 22, 3422–3448, 2009a*.

Bretherton, C.S., M. G. Flanner, and D. Mitchell (2012). Toward a minimal representation of aerosols in climate models: description and evaluation in the Community Atmosphere Model CAM5. *Geosci. Model Dev., 5(3):709–739, 2012. doi: 10.5194/gmd-5-709-2012.*

Brown, R. A. (2004). Resolution dependence of orographic torques. *Q.J.R. Meteorol. Soc., 130: 3029-3046. https://doi.org/10.1256/qj.04.21*

Bryan et al. (1996). The NCAR CSM Flux Coupler, *Technical Report NCAR/TN-424+STR, National Center for Atmospheric Research, Boulder, Colorado*.

Dai et al. (2003), The Common Land Model. *Bulletin of the American Meteorological Society, 84(8), 1013-1024. https://doi.org/10.1175/BAMS-84-8-1013*

Davini, P. and D'Andrea, F. (2020). From CMIP3 to CMIP6: Northern Hemisphere Atmospheric Blocking Simulation in Present and Future Climate. *Journal of Climate, 33(23), 10021-10038. https://doi.org/10.1175/JCLI-D-19-0862.1*

Dennis, J.M. et al. (2012). "CAM-SE: A scalable spectral element dynamical core for the Community Atmosphere Model". *In: The International Journal of High Performance Computing Applications 26.*

Gettelman, A., H. Morrison, and S.J. Ghan (2008). A new two-moment bulk stratiform cloud microphysics scheme in the Community Atmosphere Model, version 3 (CAM3). Part II: Single-column and global results. *Journal of Climate 21(15): 3660-3679.*

Hersbach, H. et al. (2020). The ERA5 global reanalysis. *Q. J. Roy.Met. Soc., 146, 730, 1999-2049, https://doi.org/10.1002/qj.3803*.

Hurrell, J. W., et al. (2013). The community earth system model: a framework for collaborative research. *Bulletin of the American Meteorological Society 94(9):1339-1360.*

Iacono M.J., J. S. Delamere, E. J. Mlawer, M. W. Shephard, S. A. Clough, and W. D. Collins (2008). Radiative forcing by long-lived greenhouse gases: Calculations with the AER radiative transfer models, *J. Geophys. Res.: Atmospheres, 113(D13). doi:10.1029/2008JD009944.*

IPCC (2013). Climate Change: The Physical Science Basis. Contribution of Working Group I to the Fifth Assessment Report of the Intergovernmental Panel on Climate Change [Stocker, T.F., D. Qin, G.-K. Plattner, M. Tignor, S.K. Allen, J. Boschung, A. Nauels, Y. Xia, V. Bex and P.M. Midgley (eds.)]. *Cambridge University Press, Cambridge, United Kingdom and New York, NY, USA, 1535 pp, doi:10.1017/CBO9781107415324*.

Jung, T., Balsamo, G., Bechtold, P., Beljaars, A.C.M., Köhler, M., Miller, M.J., Morcrette, J.-J., Orr, A., Rodwell, M.J. and Tompkins, A.M. (2010). The ECMWF model climate: recent progress through improved physical parametrizations. *Q.J.R. Meteorol. Soc., 136: 1145-1160.* https://doi.org/10.1002/qj.634

Lindvall, J., G. Svensson and R. Caballero (2017). The impact of changes in parameterizations of surface drag and vertical diffusion on the large-scale circulation in the Community Atmosphere Model (CAM5). *Clim Dyn,* ***48,*** *3741–3758.* https://doi.org/10.1007/s00382-016-3299-9.

Lindzen, R. S. (1981). Turbulence and stress due to gravity wave and tidal breakdown, *J. Geophys. Res., 86, 9701–9714.*

Liu X., R. C. et al. (2012). Toward a minimal representation of aerosols in climate models: description and evaluation in the Community Atmosphere Model CAM5. *Geosci. Model Dev., 5(3):709–739. doi: 10.5194/gmd-5-709-2012.*

Madec, G. et al (2008). NEMO ocean engine. *Institut Pierre Simon Laplace, Note du Pole de Modelisation 27, 2008. URL: http://www.nemo-ocean.eu/ content/download/21612/97924/ file/NEMO_book_3_4.pdf.*

McFarlane, N. A. (1987). The effect of orographically excited wave drag on the general circulation of the lower stratosphere and troposphere. *J. Atmos. Sci., 44, 1775–1800.*

Morrison, H. and A. Gettelman (2008). A new two-moment bulk stratiform cloud microphysics scheme in the Community Atmosphere Model, version 3 (CAM3). Part I: Description and numerical tests. *Journal of Climate 21, 15, 3642-3659.*

Neale R.B. et al. (2012). Description of the NCAR Community Atmosphere Model (CAM 5.0). *NCAR Technical Note NCAR/TN-486, National Center for Atmospheric Research.* https://www.cesm.ucar.edu/models/cesm1.0/cam/docs/description/cam5_desc.pdf .

Palmer, T.N., Shutts, G.J. and Swinbank, R. (1986). Alleviation of a systematic westerly bias in general circulation and numerical weather prediction models through an orographic gravity wave drag parametrization. *Q.J.R. Meteorol. Soc., 112: 1001-1039. https://doi.org/10.1002/qj.49711247406*

Park. S. and C. S. Bretherton (2009). The University of Washington shallow convection and moist turbulence schemes and their impact on climate simulations with the Community Atmosphere Model. *J. Climate, 22(12):3449–3469, 2009. doi:10. 1175/2008JCLI2557.1.*

Patera A.T. (1984). A spectral element method for fluid dynamics - Laminar flow in a channel expansion. *Journal of Computational Physics, 54:468--488, 1984.*

Pincus, R., H. W. Barker, and J.-J. Morcrette (2003). A fast, flexible, approximate technique for computing radiative transfer in inhomogeneous cloud fields. *J. Geophys. Res.: Atmospheres, 108(D13), 2003. doi: 10.1029/2002JD003322.*

Pithan, F., Shepherd, T. G., Zappa, G., and Sandu, I. (2016). Climate model biases in jet streams, blocking and storm tracks resulting from missing orographic drag, *Geophys. Res. Lett., 43, 7231– 7240, DOI:10.1002/2016GL069551*

Raymond, D. J., and A. M. Blyth (1986). A stochastic mixing model for non-precipitating cumulus clouds, *J. Atmos. Sci., 43, 2708–2718.*

Raymond, D. J., and A. M. Blyth (1992). Extension of the stochastic mixing model to cumulonimbus clouds, *J. Atmos. Sci., 49, 1968–1983.*

Rancic, M., R. Purser, and F. Mesinger (1996). A global shallow-water model using an expanded spherical cube: Gnomonic versus conformal coordinates, *Q. J. R. Meteorol. Soc., 122, 959–982.*

Richter, J. H., and P. J. Rasch (2008). Effects of convective momentum transport on the atmospheric circulation in the community atmosphere model, version 3, *J. Climate, 21, 1487–1499, 2008.*

Richter, J. H., F. Sassi, and R. R. Garcia (2010). Toward a Physically Based Gravity Wave Source Parameterization in a General Circulation Model. *J. Atmos. Sci., **67**, 136–156, https://doi.org/10.1175/2009JAS3112.1*.

Richter, J. H., A. Solomon and J.T. Bacmeister (2014). Effects of vertical resolution and nonorographic gravity wave drag on the simulated *climate* in the Community Atmosphere Model, version 5. *Journal of Advances in Modeling Earth Systems, 6(2), 357-383.*

Sadourny, R. (1972). Conservative finite-difference approximations of the primitive equations on quasi uniform spherical grids. *Mon. Wea. Rev., 100 (2), 136–144.*

Sandu, I., van Niekerk, A., Shepherd, T.G. et al. (2019). Impacts of orography on large-scale atmospheric circulation. *npj Clim Atmos Sci* ***2,*** *10. https://doi.org/10.1038/s41612-019-0065-9*

Sanna, A., A. Borrelli, P. Athanasiadis, S. Materia, A. Storto, S. Tibaldi, S. Gualdi (2017). CMCC-SPS3: The CMCC Seasonal Prediction System 3. *Centro Euro-Mediterraneo sui Cambiamenti Climatici. CMCC Tech. Rep. RP0285, 61pp. Available at adress: https://www.cmcc.it/it/publications/rp0285-cmcc-sps3-the-cmcc-seasonal-prediction-system-3/*

Simmons, A. J., and D. M. Burridge (1981). An energy and angular momentum conserving vertical finite-difference scheme and hybrid vertical coordinates, *Mon. Wea. Rev., 109, 758–766.*

Tibladi, S. (1986). Envelope Orography and Maintenance of the Quasi-Stationary Circulation in the ECMWF Global Models, in *Advances in Geophysics, 29, 339-374, https://doi.org/10.1016/S0065-2687(08)60045-X*.

Tibaldi, S. and F. Molteni (1990). On the Operational Predictability of Blocking. *Tellus A: Dynamic Meteorology and Oceanography, 42:3, 343-365, DOI: 10.3402/tellusa.v42i3.11882*

Tibaldi, S. and F. Molteni (2017). Atmospheric Blocking in Observation and Models. *Oxford Research Encyclopedia of Climate Science. Dynamics of Climate Systems. DOI:10.1093/acrefore/9780190228620.013.611.*

van Niekerk, A., Shepherd, T.G., Vosper, S.B. and Webster, S. (2016). Sensitivity of resolved and parametrized surface drag to changes in resolution and parametrization. *Q.J.R. Meteorol. Soc., 142: 2300-2313. https://doi.org/10.1002/qj.2821*

Vosper, S.B., Brown, A.R. and Webster, S. (2016). Orographic drag on islands in the NWP mountain grey zone. *Q.J.R. Meteorol. Soc., 142: 3128-3137. https://doi.org/10.1002/qj.2894*

Wallace, J.M., Tibaldi, S. and Simmons, A.J. (1983). Reduction of systematic forecast errors in the ECMWF model through the introduction of an envelope orography. *Q.J.R. Meteorol. Soc., 109: 683-717. https://doi.org/10.1002/qj.49710946202*

Woollings, T., Hannachi, A. and Hoskins, B. (2010). Variability of the North Atlantic eddy-driven jet stream. *Q.J.R. Meteorol. Soc., 136: 856-868. https://doi.org/10.1002/qj.625*

Woollings, T., Barriopedro, D., Methven, J. et al. (2018). Blocking and its Response to Climate Change. *Curr Clim Change Rep* ***4,*** *287–300. https://doi.org/10.1007/s40641-018-0108-z*

Zhang, G. J., and N. A. McFarlane (1995). Sensitivity of climate simulations to the parameterization of cumulus convection in the Canadian Climate Centre general circulation model, *Atmosphere-Ocean, 33, 407–446.*